6-29-2021

Automated Photometry of γ Cassiopeiae: The Last Roundup

M. A. Smith
NSF's National Optical–Infrared Astronomy Research Laboratory

Gregory W. Henry
Tennessee State University

Recommended Citation

M. A. Smith and G. W. Henry 2021 ApJ 915 13

Draft version May 6, 2021
Typeset using LaTeX **twocolumn** style in AASTeX61

AUTOMATED PHOTOMETRY OF γ CASSIOPEIAE: THE LAST ROUNDUP

M. A. Smith[1] and G. W. Henry[2]

[1] *NSF's National Optical-Infrared Astronomy Research Laboratory, 950 N. Cherry Ave., Tucson, AZ 85721, USA*
[2] *Center of Excellence in Information Systems, Tennessee State University, Nashville, TN 37209, USA*

(Received January, 4, 2021)

Submitted to ApJ

ABSTRACT

γ Cas (B0.5IVe) is the noted prototype of a subgroup of classical Be stars exhibiting hard thermal X-ray emission. This paper reports results from a 23-year optical campaign on this star with an Automated Photometric Telescope (APT). A series of unstable long cycles of length 56–91 days has nearly ceased over the last decade. Also, we revise the frequency of the dominant coherent signal at $0.82238\,\mathrm{d}^{-1}$. This signal's amplitude has nearly disappeared in the last 15 years but has somewhat recovered its former strength. We confirm the presence of secondary nonradial pulsation signals found by other authors at frequencies 1.24, 2.48, and $5.03\,\mathrm{d}^{-1}$. The APT data from intensively monitored nights reveal rapidly variable amplitudes among these frequencies. We show that peculiarities in the $0.82\,\mathrm{d}^{-1}$ waveform exist that can vary even over several days. Although the $0.82\,\mathrm{d}^{-1}$ frequency is near the star's presumed rotational frequency, because of its phase slippage with respect to a dip pattern in its far-UV light curve, it is preferable to consider the UV pattern, not the $0.82\,\mathrm{d}^{-1}$ signal, as associated with rotational modulation. We also find hints of the UV dip pattern in periodograms of seasonal data early in our program.

Keywords: Stars: individual — Stars: emission line, Be — X-rays: stars

Corresponding author: M. Smith
myronmeister@gmail.com

1. INTRODUCTION

As the prototype of the classical Be stars, γ Cas (B0.5 IVe) has exhibited a long history of multiwavelength variability, ranging from disappearance of its Be decretion disk to optical and X-ray flaring (Doazan et al. 1983; Harmanec 2002; Smith 2019a, "S19") Apart from its optical variability, it has become an object of interest among high-energy astronomers since its discovery as a hard X-ray emitter (Mason et al. 1976; White et al. 1982). Given these discoveries, γ Cas has been a target of several multiwavelength campaigns.

With a considerable X-ray flux ($L_x/L_{bol} = 3\text{-}5\times10^{-6}$), it is also the prototype of an X-ray class of at least 25 members (Nazé et al. 2020a, "N20a"). These stars are defined by their hard (but thermal) X-ray spectra, which exhibit emission lines from multiple thermal components. The spectrum of γ Cas itself indicates a dominant $kT \approx 14$ keV plasma that overwhelms fluxes at all X-ray energies. Its X-ray light curve is variable over timescales from seconds to more than a year. A peculiar, if not unique, characteristic of the apparently bright members of the class is the existence of ubiquitous rapid X-ray "quasi-flares". These features have decay times as short as 4 s, proving they are formed in photospheric densities (Smith et al. 1998a, "SRC"). A review of the properties of these unique X-ray Be stars is given in Smith et al. (2016, "SLM2016").

To bridge the optical and X-ray domains, SRC and Smith et al. (1998b, "SRH") were able to conduct a 34-hour time series with the Short-Wavelength Prime (SWP) camera of the International Ultraviolet Explorer (IUE) in 1996 January and also simultaneous 21.5 hour monitoring with the Hubble Space Telescope/Goddard High Resolution Spectrometer (GHRS) and the Rossi X-ray Timing Explorer (RXTE) on 1996 March 14-15. With the decommissionings of the IUE and GHRS, no further UV monitoring has been possible.

Several interesting results came of these campaigns, notably flux correlations between the optical and X-ray domains. GHRS spectra were binned in wavelength to construct a high SNR and high time-resolution quasi-continuum "UVC" light curve. Two prominent (∼1%) dips, each lasting a few hours and separated by about 9 hours, were visible. Photospheric UV spectral lines of Si^{2+}, Si^{3+}, Ni^{+}, Fe^{+}, Fe^{4+}, and S^{3+} in the same dataset showed correlations/anticorrelations with the UVC curve (Smith & Robinson 1999, "SR99"; Smith & Robinson 2003). These UV diagnostics were in turn correlated with the simultaneous X-ray fluxes. To add to this mix, we found the two dips separated by 9 hours observed by the IUE 57 days earlier. The same dip pattern emerged from IUE observations in 1982 found in the IUE archive. Although the $\lambda\lambda$1407–1417 GHRS light curve could not exhibit color changes during the events, the broad wavelength range of IUE/SWP spectra revealed that the color changes were consistent with absorptions by large cool clouds attached to the star over intermediate latitudes (SRH).

Another pattern in the GHRS data was short-lived migrating subfeatures *(msf)* that moved blue-to-red across line profiles. Similar features had been found in optical spectra by Yang et al. (1988) and Smith (1995). Because this phenomenon had been observed only spectroscopically for γ Cas, we were curious to see whether it also has a signature in broad-band photometry.

These patterns indicated the need for long-term monitoring of the star. Therefore, in 1997 we initiated a campaign with Tennessee State University's T3 Automated Photometric Telescope (APT). Although the APT shared observing time with several other scientific projects, we planned to observe γ Cas a few times on every available photometric night it was in view. Occasionally we could dedicate full nights to the program.

The first discovery from the APT campaign was of noncoherent, unstable "long cycles" ranging in length from about 56 to 91 days (Robinson et al. 2002, "RSH"; Smith et al. 2006 (Paper 1); Henry & Smith 2012 (Paper 2)). The amplitudes of the cycles observed in V are often larger than in B, which implies they are caused by density modulations within the decretion disk.

To see if these long cycles were related to the star's X-ray flux, RSH requested and were granted six 27-hour RXTE visits during 2000–2001. The exposure durations were chosen to average the flux over the star's estimated rotational period. Intervals between successive visits were doubled, such that RXTE covered a timescale range from a week to almost 11 months. Paper 1 reported that X-ray and optical fluxes during this interval revealed a sinusoidal fit to the APT long-cycle variations that, when suitably scaled to the X-ray fluxes, showed a very good match. They suggested that the long cycles in the optical and X-ray regimes were caused by a magnetorotational disk dynamo. The authors extended this correlation by demonstrating a reasonably good prediction of the X-ray flux from the ongoing APT monitoring. An updated APT dataset was investigated by Motch et al. (2015) using the RXTE All Sky Monitoring data as well as a later Japanese MAXI (X-ray) dataset. These authors confirmed the optical/X-ray correlation of Paper 1 and found that the APT and X-ray datasets correlated from short (a few hours) to very long (weeks or longer) timescales as well. The latter X-ray datasets were independent of the X-ray data in Paper 1. Also, these authors found that there is no visible time lag

between the two sets of variations, in contrast to lags typical of X-ray Be-NS (neutron star) binaries.

In addition to long cycles, Papers 1 and 2 reported a coherent signal with $P = 1.2158$ d ($0.82\,\mathrm{d}^{-1} \equiv$ "f_{82}"). We had noticed that this frequency is consistent with the expected rotational period of $\sim$1.24 d, according to our estimated physical parameters for the star. Thus, we adopted 1.21 d as the rotational period. Similarly, we suggested that the periodic UVC dips were caused by rotational modulation of anchored clouds. This paper will revisit these findings.

2. A SKETCH OF SUGGESTED X-RAY MECHANISMS

As it is relevant to the APT study, we sketch a history of attempts to explain the production of hard, thermal X-ray flux in γ Cas and its association with certain optical and UV variabilities.

Harmanec et al. (2000) discovered that γ Cas is a binary system. Its orbital period is 203.5 d, and it is in a nearly circular orbit ($e \lesssim 0.03$). Although the secondary's mass is $0.9 \pm 0.1 M_\odot$ (Nemravová et al. 2012, Smith et al. 2012 "SLM"), its evolutionary status is unknown. However, the evidence is strong that the Be star is a blue straggler (Mamajek 2017a, 2017b) and therefore probably has an envelope-stripped or degenerate secondary. Assuming the secondary's mass estimate is accurate, the mass is too low for it to be a NS, but it is appropriate for a white dwarf (WD) and (envelope-stripped) helium stars. The limit straddles the masses of sdO stars.

Wang et al. (2017) have cross-correlated IUE spectra of γ Cas but found no evidence of a far-UV contribution in the far-UV down to a level of 0.6%. This result rules out a range of types of evolved, low-luminosity companions. However, Wang et al. (2021) performed the same tests on 13 other early-type Be stars not previously known to be in binaries and found 10 from this sample exhibit at least traces of a spectrum of a hot subluminous secondary such as an sdO star. Using the same technique, Gies et al. (1998) and Peters et al. (2008, 2013, 2016) had previously discovered substantial UV contributions from sdO secondaries of three Be binaries (ϕ Per, FY CMa, and 59 Cyg). In a fourth case, HR 2142 only a faint contribution can be seen from a "sdO in transition." Clearly, sdO's are the most likely kind of secondary in early-Be systems. Thus, to see if these sdO's could be seen against γ Cas as the primary star, we substituted the appropriate physical parameters of γ Cas for the parameters of the actual primaries and recomputed the secondary flux contributions to simulated γ Cas-sdO systems. This exercise confirmed that sdO contributions would still be recognizable for the first three imaginary cases if γ Cas had been the primary. We add finally that at least two of the binaries in the Peters-Gies et al. sample, 59 Cyg and ϕ Per (those with the brightest and most massive hot secondaries) are faint and soft X-ray systems (Nazé et al. 2020a, HEASARC Rosat Data Archive2020), which clearly cannot be confused with γ Cas star emissions.

Even before the binarity of γ Cas was discovered, accretion of Be wind onto a degenerate object was suggested as the source of the hard X-ray emission. White et al. (1982) and Murakami et al. (1986) had argued that a secondary ought to be a NS or WD. More recently, various authors have again suggested accretion involving degenerate or hot secondaries: a WD (Hamaguchi et al. 2016), a NS in propeller stage (Postnov et al. 2017), or interactions between an sdO wind and the Be disk (Langer et al. 2020, "L20").

Difficulties described by SLM16 in reconciling the unique X-ray characteristics of γ Cas with those of other X-ray classes of Be stars motivated SRC, SR99, and Robinson & Smith (2000, "RS00") to advance a very different mechanism for the hard-X-ray production: the star-disk magnetic interaction hypothesis.

This idea requires the tangling of field lines from putative small-scale magnetic surface complexes (e.g., Cantiello & Braithwaite 2011) and a toroidal field in the inner decretion disk. The different angular rotation rates of the star and the disk cause interactions of star-disk fields, which in a short time entangle, break, reconnect, and ultimately relax. This process releases magnetic energy, which accelerates embedded particles in high-energy beams. Some of these are guided by protruding surface field lines toward the star. In fact, the existence of downstreaming matter can be inferred from highly redshifted absorption lines in the 1996 March GHRS time series (SR99). According to simulations by RS00, nearly monoenergetic (200 keV) electron beams impact and thermalize at the surface, causing local explosions (also called "flares"). Their detritus accumulates in low-density canopies and decays in $\sim$20 mins, producing a basal flux of the same high temperature.

3. OBSERVATIONS

We have been conducting Johnson B and V photometric observations of γ Cas since 1997 with the T3 0.4 m APT facility at Fairborn Observatory in southern Arizona (Henry 1995a, b, Henry 1999, Eaton et al. 2003). The APT acquires successive brightness measurements of individual target stars with a single-channel photometer using a temperature-stabilized EMI 9924B photomultiplier tube. Each observation of γ Cas, which we

refer to as a *group* observation, consists of the mean of three B and V differential measurements of γ Cas with respect to its comparison star (HD 6210) and the mean of two measurements of the check star (HD 5395) with respect to the comparison star.

To avoid saturating the detector on 2nd magnitude γ Cas, we used a 3.8 mag neutral density filter to observe all three stars, with the exception of the 1997 season when we used different neutral density filters for γ Cas and the comparison stars.

γ Cas comes to opposition in early October, and our APT observing seasons always covered the months of September through early February. Telescope closure was generally forced by Arizona's summer monsoons. However, if the monsoons arrived late, a new season included some nights in June-July. In the analysis that follows, we label each season by the year corresponding to the star's opposition. Our final dataset covers 23 consecutive observing seasons from 1997 through 2019.

On most clear nights the APT was programmed to acquire 1–4 observations spaced by $\geq$2 hours. During most observing seasons, a few nights near opposition were dedicated to monitoring for several hours. On those nights the APT acquired 1-4 group observations spaced about 8 minutes apart. On good nights the external precision of the group means was typically 0.003–0.004 mag, as determined from observations of pairs of constant stars. Since the APT can acquire observations in marginal photometric conditions, we rejected as outliers any group mean differential magnitudes with standard deviations greater than 0.01 mag. Because we used different neutral density filters for the variable and comparison stars in the 1997 season, we were forced to adjust those means to the 1998 season means. Finally, the check minus comparison star differential magnitudes demonstrated that both are constant to $\leq$0.005 mag on seasonal and year-to-year time scales.

In this paper we present our final 1997–2019 dataset for γ Cas, consisting of 5554 observations in the B and 5488 in the V passbands. We have cleaned the dataset by fitting sine curves to the long cycle ($\sim$70-80 day) variability in single observing seasons and rejected as outliers those observations with residuals from the least-squares sine fit of $\geq 2.5\sigma$. For several of the later observing seasons, where we could not obtain a reliable long cycle, we rejected observations that were $\geq 3.0\sigma$ from the seasonal mean magnitudes.

Our analysis technique employed the frequency-search method of Vaníček (2001), based on least-squares fitting of sine curves, to search for periodicities in various combinations of the yearly photometric datasets. This method uses the reduction factor in the data's variance as a goodness-of-fit parameter. For all analyses we initially scanned trial frequencies over a range 0.005–6.0 d^{-1}. Formal uncertainties in the best-fit periods and amplitudes were computed from standard propagation formulae. We consider a signal to be real only if it is found in both B and V datasets. For multiseasonal analyses we forced the seasonal means to the same value to eliminate those low-frequency variations that can be seen in the long-term light curve (Fig. 1). If $>3\sigma$ outliers were present at any of the frequencies detected within the individual observing seasons, we removed those observations from our dataset and recomputed all frequencies for that season. In total, we rejected $\approx$6% of the observations acquired by the APT. The total number of observations given above are the observations that survived analyses of the individual observing seasons. These data are listed in Table 1. The full table is given on the VizieR website accompanying this paper. The mean V and $(B-V)$ magnitudes in the Johnson system are $< V >$ = 2.165 and $< B-V >$ = -0.083.

Table 1. Automatic Photoelectric Telescope Observations of γ Cas (Seasons 1997-2019)

Date (RJD)	Var B (mag)	Var V (mag)	Chk B (mag)	Chk V (mag)
50718.6953	-4.306	-3.671	-0.809	-1.213
50718.9258	-4.306	-3.672	-0.805	-1.219
50720.7930	-4.299	-3.674	-0.812	-1.215
50720.9180	-4.300	-3.668	99.999	-1.220

Note: (Stub.)
The full dataset may be retrieved from the Journal's VizieR website for this paper. A value of 99.999 indicates the differential magnitude had an uncertainty >0.01 mag and was rejected.

4. RESULTS

4.1. *The full light curve*

The B differential magnitude dataset is plotted in Fig. 1. Besides short-term brightness variations, the plot exhibits a sinuous character over a range of $\sim$0.05 mag in the 23 seasonal means. The bottom curve shows that the $B-V$ color index is reddened by 0.04 mag during this time, though not in strict correlation with B (or V) magnitudes. Because there is no other plausible source of surplus red continuum flux in the γ Cas system, we may assume that the variable reddening results from changes in disk extent and/or density. However, we also notice the unusual variations occurring between Seasons 2018 and 2019 when the B flux has decreased and the V flux decreased too, but less so. It is possible that the

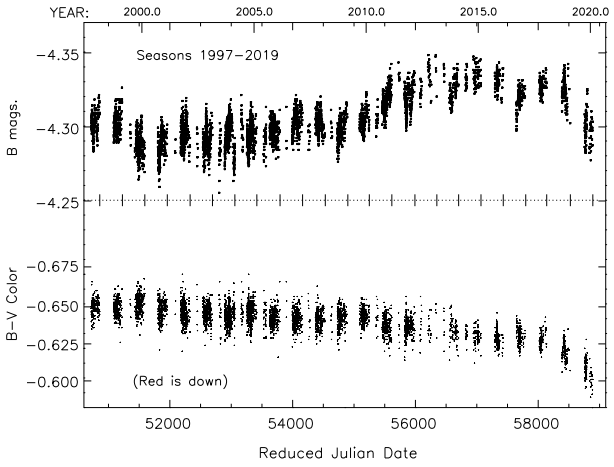

Figure 1. The APT B and $B-V$ magnitudes for the γ Cas program for Seasons 1997–2019. Tick lines mark each season's end. The brightening and reddening segment after RJD 55400 marks an outburst during 2010-2011. In the last season the $B-V$ color reddens because the Be star fades more in B than in V.

disk has developed enough in this time that it has become opaque even in the blue. Then, assuming the inner disk edge occults part of the star, its enhanced optical thickness will dim the combined star/disk light even in the B passband.

4.2. *Long cycles*

Table 2 lists by APT season the numbers of B and V observations and the lengths of the long cycles. These are taken from Papers 1 and 2 and, from Season 2012 on, new observations. As previously noted, the waveforms for the long cycles are not always sinusoidal. They can grow, damp out, or exhibit a net trend. At times they "morphed" to a new quasi-period within two weeks or less. Errors in the long-cycle lengths were estimated in Papers 1 and 2 to be ±1 day for simple sinusoids to ±2 days for damped cases. In contrast to Paper 2, the full (peak-to-peak) amplitudes we list in Table 3 were computed by sinusoidal fits and without (sparce) summer observations. Thus the amplitudes here are not identical to those in the previous papers. The errors in cycle amplitudes are likewise dependent on the character of the variations and therefore also difficult to assign. We estimate them conservatively to be $\pm15\%$ (see Fig. 2). The full-amplitude detection threshold is about $\sim$1 mmag.

From the seasonal history of the long cycles given in Fig. 2 and the table, their character appears chaotic, offering no obvious predictive power or memory of previous cycles. Following the cycles' decline in 2012-2013, one sees that they may have recovered slightly in Seasons 2018–2019. This is at least consistent with the long-period, meandering character of the TESS satellite[1] observations during this season, which further supports this general picture.

Table 2. Summary of APT Observations with long period and f_{82} properties

Season	# Obsns. B/V	Long Cycle "Periods"	Long Cycle B/V Ampls.	f_{82} B/V Ampls.
1997	179/183	61	14.0/15.9	4.4/4.4
1998	206/209	65	6.8/7.6	5.9/6.1
1999	254/251	72	14.1/14.9	4.8/6.1
2000	290/290	91	14.8/17.6	3.4/6.1
2001	332/327	73	10.6/11.9	7.1/6.4
2002	300/300	80	16.4/21.0	7.6/4.7
2003	659/655	90:	19:/21:[3]	6.3/7.2
2004	647/641	85	11.2/15.8	3.6/2.7
2005	287/275	66	6.0/4.9	5.3/2.6
2006	266/270	88	13.3/17.6	0.6/2.3
2007	254/248	88	11.2/13.9	0.8/2.0
2008	245/242	60	10.8/9.3	2.3/2.0
2009	192/188	70	10.2/9.3	0.7/1.5
2010	278/278	72	13.2/19.1	1.8/2.8
2011	326/318	73	17.7/20.1	1.5/2.0
2012	40/34	70	10.1/18.3	0.0/0.0
2013	93/93	–	–	1.4/0.0
2014	91/89	–	–	3.3/3.4
2015	132/126	–	–	3.4/2.9
2016	173/169	–	–	2.5/3.0
2017	87/88	–	–	2.2/0.0
2018	120/113	56	1.8/1.0	2.1/1.6
2019	103/101	73	1.6/1.9	1.5/2.4

Notes: (1) For conciseness B and V properties are separated by a slash symbol.
(2) Full amplitudes are in mmag; cycle lengths in days.
(3) Paper 1 showed damping/regrowth of cycle amplitude.

4.3. *Confirmation of f_{82} and other signals*

4.3.1. *Search procedure*

[1] The Transiting Exoplanet Survey Satellite (TESS) (Ricker et al. 2015) was launched by NASA in 2018 to survey the sky with broad-band optical photometry. The time cadence for γ Cas observations was 30 mins.

Table 3. Signal frequencies (d^{-1}) and full amplitudes (mmag)

Multiseason	0.82	1.24	2.48	5.03
Paper 1:				
1997-2004 (B)	0.82245	1.24310	2.47944	5.02903
Full ampl.:	5.92±0.35	3.00±0.37	1.53±0.38	3.00±0.38
1997-2004 (V)	0.82244	1.24304	2.47937	5.02328
Full ampl.:	6.80±0.39	3.30±0.42	1.66±0.42	3.31±0.42
Paper 2				
2005-2011(B)	0.82929	1.24171	2.47975	5.03873
	2.28±0.45	2.11±0.45	2.23±0.45	1.54±0.46
2005-2011(V)	0.81929	1.26146	2.47980	5.02477
	2.47±0.45	2.36±0.49	1.70±0.49	1.34±0.50
New data:				
2012-2019 (B)	0.82394	1.24263	2.47946	5.03244
	2.32±0.65	1.58:/2.37±0.65	3.49±0.64	2.25±0.66
2012-2019 (V)	0.82762	1.25951	2.46901	5.02552
	2.46±0.67	2.00±0.68	2.44±0.65	2.54±0.66
23 seasons[3]	0.82238(10)	1.2448(19)	2.481(11)	5.027(20)
(B)	3.51±0.29	1.89±0.29	2.42±0.39	3.00±0.38
(V)	3.58±0.28	2.20±0.29	2.15±0.50	2.60±0.41
f_{82} ephemeris				
from 23 seasons:	$T_\circ$: (RJD)	P (d):	f_{82}	
B	51086.602	1.215975	0.822385	
V	51086.612	1.215987	0.822377	
Avg. $T_\circ$, P, f	51086.607(5)	1.21598(1)	0.82238(1)	

Notes: (1) The 1.21 d (f_{82}) ephemeris is: $\phi = (T - T_\circ)/2\pi P$;
(2) $\phi = 0.0$ refers to the "faint star" phase;
(3) The last digit in both the amplitude and frequency is not significant.

Our search procedure for coherent frequencies was first to run our Vaníček periodogram generator through a broad frequency range for each season (and each filter) and to tabulate the formal errors in the amplitudes of all significant peaks. This procedure worked well for f_{82} and for all but one of the signals we may have found (see reference to 0.76 d^{-1} in §4.3.3).

We digress to point out that in their analysis of the TESS light curve of γ Cas during Sectors 17, 18, and 24, Labadie-Bartz et al. (2021, "LB21") have discovered a low-amplitude group of NRP modes, which they designate as "group g_1." However, their amplitudes are too low to be detectable by the APT, and they flutter on an unknown timescale. The more stable, and larger-amplitude f_{82}, first noted in the APT light curves of Papers 1 and 2, occurs at the low frequency edge of the g_1 group. Because these modes are so weak and well separated from aliases associated with the APT observing windows, we believe they are not directly related to f_{82}.

In Paper 2 we found that uncertainties in the full amplitudes for single seasons range from ±1.0 to ±1.5 mmag. After analyzing the individual seasons, we ran searches on three groups of seasonal datasets: early, middle, and late (see Table 3), according to the seasons added to Papers 1, 2, and this work. Initial amplitude errors were formal ones, as propagated from the Vaníček analysis. The errors for multiseasonal periodograms are lower than the single-season errors. The 23-season errors were calculated in the same matter.

To assess the effect of hypothetically fewer observations than were made, we split our database in two,

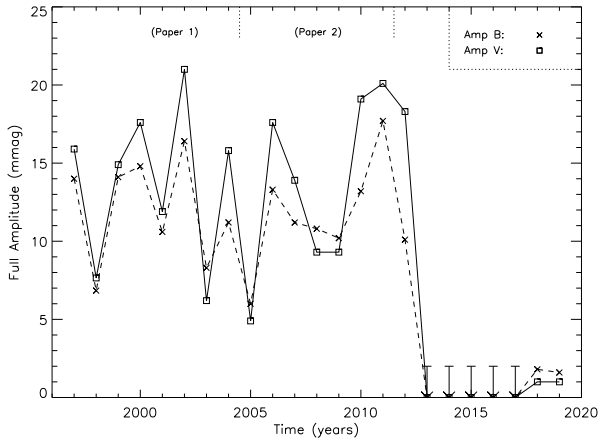

Figure 2. The seasonal APT history of long-cycle full-amplitudes of γ Cas. Solid and dashed lines and symbols annotate filter. The seasons covered by Papers 1 and 2 are indicated. For most of the last several years the amplitudes have been too small to detect.

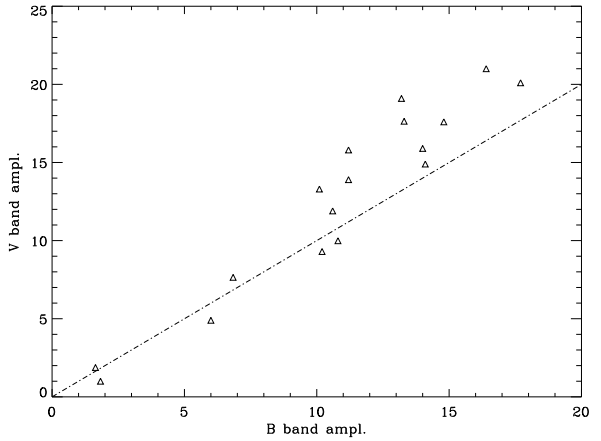

Figure 3. The correlation of B and V amplitudes in mmag from the long-cycle history in Fig. 2. For amplitudes greater than 10 mmag the V amplitudes become significantly larger than in B, demonstrating that the origin of these variations is the Be disk.

each comprised of even or odd-numbered points, and reran our 23-season analysis on four discovered frequencies discussed below. As might be expected, the solutions for frequencies and amplitudes typically bracketed those computed from the full dataset. The computed r.m.s. values based on the even minus odd observation differences varied between 1 and $1\frac{1}{2}$ times the r.m.s. of the full-set solutions. In the lower ("23 seasons") panel of Table 3 we have replaced the errors of the Vaníček solutions with those from the even/odd comparisons in cases where they were larger. We also note that the amplitudes computed in the even/odd analyses fluctuated apparently randomly; there was no trend to smaller or larger values.

We repeated these trials four times by computing results for every *fourth* observation for these frequencies. About half these trials settled on the correct frequency, within the error windows given in Table 3. In the other cases a false peak (usually one of the adjacent annual aliases) was chosen, since the correct peak often did not stand out above them. With such a high failure rate as this, it was clear that we had reached the limit of our ability to detect astrophysical signals.

4.3.2. *Discovery of coherent signals*

The time history of f_{82} full-amplitudes found in APT data is given in Fig. 4 (values for 1997-2011 are from Paper 2). Although this signal was strong in early seasons, the amplitudes have decreased significantly after 2004-2005 to being barely visible until 2013 or 2014. From concurrent SMEI observations, Borre et al. (2020, "B20") reported a similar decrease in the f_{82} amplitude. It appears to have partially recovered in the following few years, but it is not visible in the later periodogram obtained during TESS Sector 17-18 (2019-2020) observations (Nazé et al. 2020c, "N20c"). According to Fig. 4, we cannot attest to the nonzero values for Seasons 2017-2019.

The lower panel of Table 3 gives our f_{82} ephemeris for all the data in both filters. The agreements between the f_{82} 23-seasons frequency for Seasons 1997–2019 and the three multiseason segments suggest that this frequency has been coherent from when the APT monitoring began in Season 1997 through Season 2011 and probably into some late seasons. Our revised frequency reduces the discrepancy between the values reported in Paper 2 and B20 ($0.82247\,\mathrm{d}^{-1}$ vs. $0.82215\,\mathrm{d}^{-1}$) by $\frac{1}{3}$. These values now differ by close to 1.0 cycle over their timespan. It is likely that either they or we have miscounted by one cycle over the span of several thousand.

Other than $0.82\,\mathrm{d}^{-1}$, we found multiseasonal signals near frequencies $1.24\,\mathrm{d}^{-1}$, $2.48\,\mathrm{d}^{-1}$, and $5.03\,\mathrm{d}^{-1}$, very similar, though not always identical to, results by B20, N20c, and LB21. Periodograms for frequencies surrounding these values are exhibited in Fig. 5, and relevant parameters for them are listed in Table 3. The $2.48\,\mathrm{d}^{-1}$ signal seems to be a robust frequency for most, if not all, of the APT observing seasons. The $5.03\,\mathrm{d}^{-1}$ and $1.24\,\mathrm{d}^{-1}$ signals require additional notes.

N20c determined a peak value of $5.054\,\mathrm{d}^{-1}$ for $f_{5.03}$, which lies at our frequency error limit. Our periodogram for this signal shows evidence of stronger annual and daily aliases than the others. In marginal detection cases

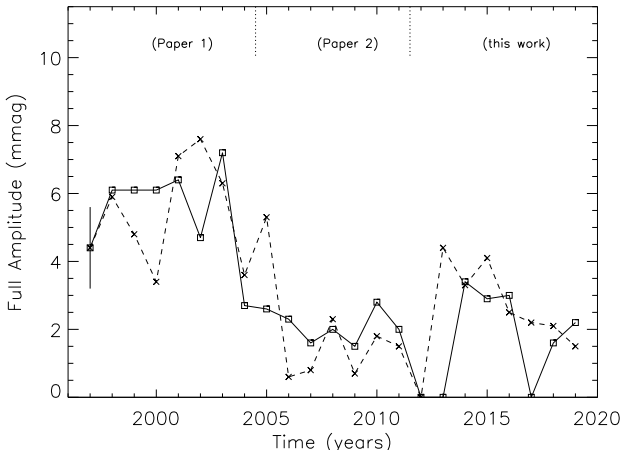

Figure 4. The time history of the seasonal full amplitudes for the f_{82} signal for B (X symbols) and V (squares) datasets. Errors for the amplitudes of ± 1.2 mmag are averages of seasonal values given in Paper 2.

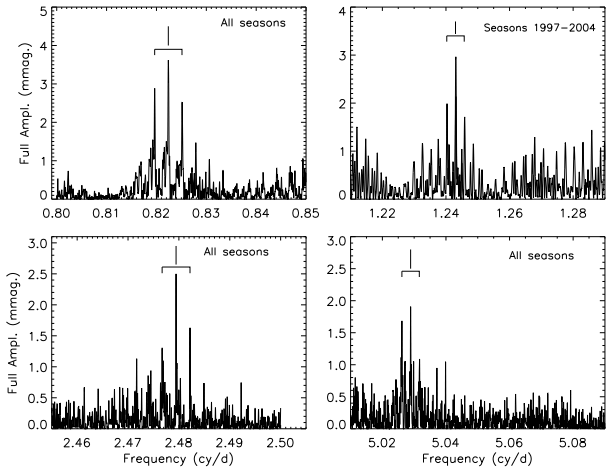

Figure 5. The B filter full-program periodograms for the four frequencies found for most of the APT seasons covered in this paper. The comb astride the vertical line denoting these frequencies highlights the ± 1 annual aliasing pattern.

like this, these may be due to the frequency's proximity to the diurnal harmonic at $5.0\,\mathrm{d}^{-1}$.

The $f_{1.24}$ signal (B20's $f_{1.25}$) was the most problematic to characterize. The filter-to-filter disparity in its amplitudes is large compared to results for the other signals, making our late seasons' solutions for it less reliable. Indeed, this signal weakened in seasons after 2004. Moreover, we suspect its amplitude was generally highly variable. For example, N20c state that in the TESS Sectors 17-18 they found "no trace" of B20's $f_{1.25}$. Yet, $f_{1.24}$ and $f_{2.48}$ signals were both present but variable at least for a few days during the beginning of Sector 18, as seen in their Fig. 6 light curve. Finally, for this event or other times, we did not find that the APT or TESS amplitudes of the two frequencies change together, as would be expected if the two were related through a harmonic resonance.

We searched our periodograms for additional signals (for example, the weak signal at $7.57\,\mathrm{d}^{-1}$, found by N20c in a TESS light curve) but detected none. In addition to the semi-stable frequencies just noted, we will cite a short-lived frequency in §4.3.3 and discuss an intermittent one in §4.6.

Before proceeding further, notice that there is no correlation between the amplitudes of the long cycles and the f_{82} signal. We note also that according to Table 1 and Pollmann (2021), the disk of γ Cas has been building since 2000 through early-2021. In the middle of this interval, γ Cas underwent a Be outburst in 2010–2011 showing increased optical continuum and Hα line brightening. As reported in Paper 2, during the initial few weeks of this outburst, an accelerated brightening of the optical continuum, $B-V$ reddening, and Hα emission occurred, which was accompanied by increased absorption in the soft X-ray region (SLM). In contrast, the near disappearance of f_{82} *preceded* the 2010 outburst by some five years and therefore was unrelated to that event. Thus, contra LB21, it is not clear that this event was associated with changes in strength of dominant nonradial pulsation (NRP) modes.

4.3.3. *Rapid amplitude changes of coherent signals*

The full amplitudes listed in Table 3 are values averaged over several seasons. From our short intensive-night campaigns (up to $7\frac{1}{2}$ hrs per night), we found that the amplitudes can vary unexpectedly. An important result coming out of our intensive monitoring on short order is that the normally dominant signal at f_{82} was sometimes eclipsed by another, nominally secondary, signal. Table 4 summarizes the results of several intensive mini-campaigns and the secondary frequencies (full amplitudes) they exhibited. Because we sometimes found temporarily dominant frequencies during these brief campaigns, their short-term behaviors suggest that their amplitudes vary much more frequently than we would infer from periodograms drawn from a full season or longer. Perhaps this "flutter" of signals is typical.

We discuss the results from our short dedicated-night campaigns season by season as follows:

Season 2000: This season included two pairs of intensive monitorings (each separated by 2-3 nights) spaced a month apart. Taking the second pair first, their variations could be fit with a signal of $f = 5.03\,\mathrm{d}^{-1}$ and a

Table 4. Results summary of intensively observed nights

Season	# Nights	Freq.	Ampl.	Comments
2000	4	5.03	6	fits last 2 nights
2001	2	0.82	7	
2003	6	0.82	11	waveform change
2004	3	1.24(?), 0.82	12	evolving freqs.
2011	1	–	<2	flat over 5 hrs
2016	2	2.48	18	

mean full-amplitude of 6 mmags. The behavior of the data in the first pair was decidedly different, exhibiting only small variations during their 4-4$\frac{1}{2}$ hr coverages.

The B, V periodograms for the whole Season 2004 exhibited peaks of amplitude 4.8-5 mmag at 1.243 d^{-1}, as well as a strong transient signal (amplitudes 5-7 mmag) at a frequency of 0.76 d^{-1}, in addition to the neighboring f_{82}. Though apparently real, this transient did not recur for any other season, and so we have not listed it in our tables as a multiseasonal signal.

Season 2001: The f_{82} full amplitude over two consecutive nights, 7 mmag, is typical for the season (Table 2).

Season 2003: Amplitudes of all three secondary frequencies were low or invisible during this season, signifying that the waveform changes discussed in §4.5.2 are unlikely to be due to intermode beating.

Season 2004: Light curves for a sequence of three consecutive nights were conspicuous with f_{82} appearing to beat with a sinusoid consistent with $\approx$1.2 d^{-1}. The combined full amplitude was large (12 mmag).

Season 2011: No variations were found over 5 hrs.

Season 2016: The observations of these two consecutive nights are the only ones observed when the 2.48 d^{-1} signal was dominant. Its amplitude then is among the largest found during all our monitoring of γ Cas.

We temper these descriptions by noting that our fittings of large-amplitude sinusoids to data of only several hours of a few nights cannot be differentiated in general from beating by roughly similar modal amplitudes. The best single case for an amplitude waxing and waning within 1–2 weeks is discussed just below.

To summarize, from the well-observed nights referred to in Table 4, one sees frequent changes in amplitudes not only for f_{82} but also for the "secondary" signals near 1.24 d^{-1}, 2.48 d^{-1}, and 5.03 d^{-1}, all probably occurring on rapid timescales. It is not surprising to find in γ Cas what are evidently NRP modes excited in this frequency range, as it is a star situated at the hot edge of the β Cep domain. Although the f_{82} amplitude starts to decrease in 2005–2012, and is generally mimicked by $f_{1.24}$ and $f_{5.03}$, the amplitude of $f_{2.48}$ increases during later seasons (Table 3.)

4.4. *Searches for other frequencies*

High frequencies ($> 8\,d^{-1}$) are of interest to this study because of their potential identification with NRP p-modes and in turn as a possible cause of the *msf* in line profiles (Nazé et al. 2020b, "N20b"). However, the quality of our APT periodograms deteriorates above 8–10 d^{-1} and is meaningless beyond it. However, N20c's published TESS periodograms for Sectors 17 & 18 exhibit no signal in the range above 8 d^{-1} out to 20 d^{-1}, (just as LB21's periodograms show no high-frequency signal down to <0.1 mmag, not only for this time period but also during Sector 24).

4.5. *Changes in f_{82} waveform*

4.5.1. *Rationale for analysis*

In Paper 1 we discovered an unusual skewness in the mean waveform of the f_{82} signal taken from the first several APT seasons. For convenience we characterized departures from a sinusoid by parameters e and ω taken from the familiar Lehmann-Filhes equation for orbital solutions of radial velocity variations. Here e and ω are a fake "eccentricity" and "longitude of periastron," respectively. Parameter e represents the waveform's pointiness while ω quantifies its skewness. Values in the fourth quadrant signify a depressed positive-phase wing; the first quadrant gives the opposite skewness. In our implementation of past and current work, we used a generalized least-squares algorithm by Markwardt (2011) adapted for our computations. For the first eight seasons (Paper 1), the resulting means, averaged over B and V filter datasets, were $e = 0.35$ and $\omega = +285°$. In Paper 2 we examined data for six dedicated and consecutive nights of observations in Season 2003 and found for the V filter that e had increased to 0.51±0.05 and the skewness had reversed sign to ω=+25°±6°. As noted then, nearly identical values and errors were found in our data by Dr. Fekel using an independent algorithm. The departures from a sinusoid is a remarkable result and thus requires confirmation. We note for completeness that the periodogram for these six nights' data exhibits a faint second harmonic feature.

To check the statistics in a different way, we conducted an experiment adopting a simple Monte Carlo strategy for the V-band dataset of another observing season, 2001, and compared errors derived for e and ω from fake datasets using the 2001 observation times and photometric errors. We then compared them with re-

sults from a direct analysis of Season 2003 data. Note that an assessment of fluctuations of both seasons's target and check-minus-comparison star data (outliers removed), revealed no significant departures from Gaussian distributions.

Our experiment began by phase-folding the Season 2001 V-band data to the f_{82} ephemeris. The best (though mediocre) sinusoidal fit was computed for these initial data, and this sinusoid was subtracted, resulting in an initial data fluctuation array. We then conducted mock data simulations for 11 independent trials by shifting the fluctuation array by phase increments of N×28 points according to each point's former position. Here N = 0, 1, 2,...,10 corresponds to trial number and 28 is an arbitrary value, which brings each point to a different observation time and night. For each trial, fluxes of the so-shifted fluctuation array were added back to the initial fitted sinusoid, and e and ω were solved for again. Finally, their means and r.m.s. errors from these trials were computed and compared with the original e and ω computed for Season 2001. The mean values turned out to be nearly coincident with the solution for the original Season 2001 data, namely means of $e = 0.16$ and ω=310° and r.m.s. errors of $\sigma_e = \pm 0.077$ and $\sigma_\omega = \pm 8°$.

We repeated this exercise by sampling only every other observation. The new r.m.s. values were $\sigma_e = \pm 0.102$ and $\sigma_\omega = \pm 12°$ and thus scaled approximately with the inverse square root of the number of points. Applying the same scaling for like-quality and increased numbers of observations to Season 2003 (Table 2), we were able to predict errors of $\sigma_e = \pm 0.055$ and $\sigma_\omega = \pm 6°$. These error estimates are nearly the same as Paper 2's results from a direct analysis of Season 2003 (viz., ±0.05 and ±6°). We will now use this result in the foregoing analysis of data subsets of this season.

4.5.2. Season 2003 waveform changes

We proceeded to analyze the waveform for B as well as V-band observations of our six intensively monitored nights from Season 2003 (Reduced Julian Day 52,962–52,967). We will then contrast it to observations taken from the rest of the season. In comparison to Paper 2's analysis, we incorporated differences in outliers comprising the seasonal dataset and used different procedures for prewhitening of the long period in this analysis. We remind the reader that we had found amplitudes from the secondary signals to be low or absent in this season.

To examine the waveform differences during this season, we used the fact that the six intensively monitored nights occurred in the middle of the observing season. We divided the datasets for the non-intensively observed nights into two halves and compared the resulting waveforms of all four groups – viz. first-half, second-half, both halves (all nonintensive nights), and the six intensive nights. The e, ω parameter determinations for these groups are given in Table 5. The most obvious result is that the full amplitude doubled from 5–6 mmags to ∼11 mmag, and then decreased to its former value. Also, the "eccentricity" for the six nights increased to 0.50 and 0.47 for B and V, respectively. This increase in e, +0.16, is more than double the predicted σ_e of ±0.055, according to our control results for Season 2001 (when scaled for numbers of data points).

Table 5. Lehmann-Filhes waveform parameters, Season 2003

Filter	Halves 1+2	(All but	6 nts.)	Intensive	(Only	6 nts.)
	Ampl.	e	ω	Ampl.	e	ω
B	5.2	0.41	348°	12.1	0.50	+20°
V	4.2	0.41	307°	10.2	0.47	+19°
	Half 1			Half 2		
	Ampl.	e	ω	Ampl.	e	ω
B	5.5	0.34	350°	5.7	0.43	340°
V	5.1	0.39	340°	5.1	0.41	319°

Note: The set of six "intensively" monitored nights occurred between two nearly equal time segments during this observing season.

These differences are visible in the phase-folded plot, Fig. 6. Here the Lehmann-Filhes fit to the six-night, B-filter data points is displayed as a solid line. We can contrast it with the Lehmann-Filhes fit to the data for all other nights in the season (dashed line) and also with the best, though mediocre, sinusoidal fit to the data for these other nights (dot-dot-dashed line). The differences between the values of e and ω and the published values in Paper 2 are comparable to the error estimates found in our control: $e = 0.50$ here vs. 0.55 in Paper 2, and $\omega = +19°$ here vs. 25° there. Also, just as with the eccentricity, its skewness subsequently reverted to its typical fourth-quadrant sense.

4.6. *The UV continuum dips*

Although the two IUE UV light curves of γ Cas lasted longer, the GHRS series of 1996 March 14-15 is unmatched in its precision. In Fig. 7 we have exploited this fact and the f_{82} ephemeris to represent this signal as a 6 mmag sinusoid (dotted line) against the GHRS data (first full curve). The error in the phase-positioning of the sinusoid is ±0.01 cycles. We have subtracted the

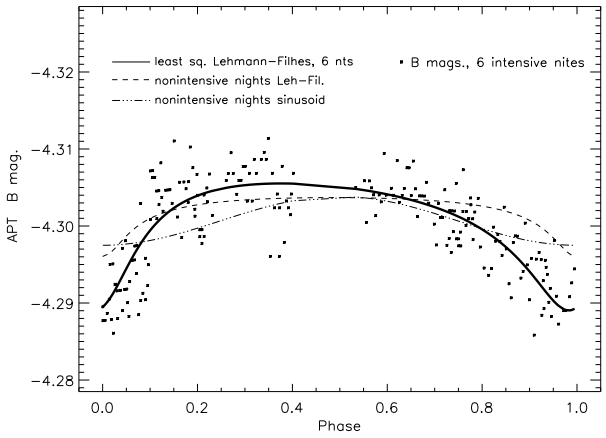

Figure 6. The waveform determined by least-squares fit to the Lehmann-Filhes solution for the B-filter, f_{82} phase-folded data for six intensively monitored nights in Season 2003 (heavy curve and dots). Note the departure of the data and this curve from the sinusoidal fit (dot-dot-dashes) and the Lehmann-Filhes fit (dashes) for the nonintensive nights: the 6-night solution has a larger amplitude and exhibits a "pointy/bowed" form and skewness with a steep negative-phase wing.

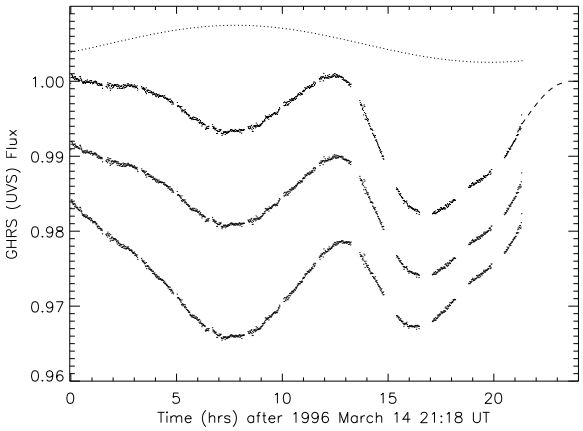

Figure 7. The GHRS UV continuum light curve of 1996 March 15 (upper full curve). The top line (dotted sinusoid) is the f_{82} signal from its ephemeris of Table 3. The second and third curves are the original GHRS curve with the top sinusoid subtracted by a factor of one and 2.5, respectively. One or the other of the lower curves shows how the undistorted UVC should appear if no f_{82} signal existed.

sinusoid from it to show how it would look if f_{82} were not present (second full curve). This would be appropriate, for example, if f_{82} is a very low-frequency, "classical" NRP g-mode, for which geometric distortion of the star would dominate flux variations. The amplitude of

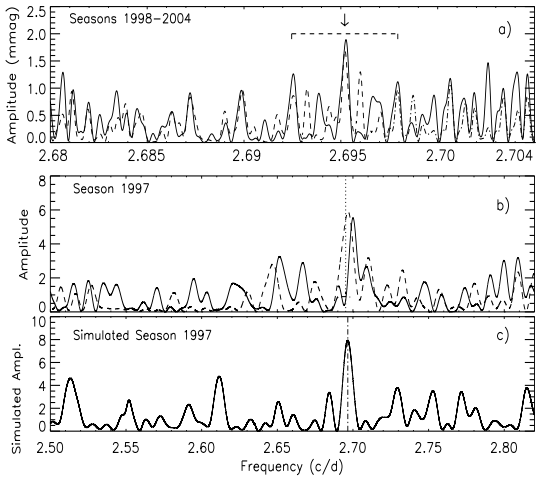

Figure 8. Periodograms for B (dashed line) and V (solid line) covering a weak signal at the expected frequency $2.695\,\mathrm{d}^{-1}$. Panel a): results for Seasons 1998–2003. The horizontal line and markers indicate the feature's annual sidelobes. Panel b): the same feature for just Season 1997. Panel c): the simulation of the GHRS signal applied to Season 1997 (see text). For Panels b) & c) we extend the frequency range to 2.5-2.82 d^{-1} to show the noise level. (The slight positional differences of the signal is not significant.) The dotted line in Panel b) is the extension of the signal arrow in Panel a). This position is almost identical to the dot-dashed line (Panel c).

the variations would then be wavelength-independent. If instead, and as argued by SRH, the absorptions arise from a cool intervening cloud, then the wavelength dependence grows in the far-UV, and the GHRS light curve will approximate the lower curve. In any case, the lower curve gives an approximation of a sinusoid, for which least-squares fitting gives a dip separation of 8.90±0.02 hr ($2.70\pm0.01\,\mathrm{d}^{-1}$). However, it is easy to show from the 1982 and 1996 IUE records, and even the GHRS curve, that these variations are not part of a true sinusoidal signal. Even so, S19 pointed out that the 43 hr-long IUE sequence suggested the presence of a third dip that seems to be the recurrence of the first dip from one rotation cycle earlier.

One can ask whether the 8.9-hr separated dips are coherent enough through the years to be detected in the APT data, since the program started just over one year after the GHRS campaign. Yet even if it was present, it is not a continuously repeating sinusoidal signal. An intermittently occurring dip will cause the periodogram to show a more complicated beating structure. Fortunately, because we now know where to isolate a narrow search range, we can search a periodogram for a peak that emerges at a predicted frequency of $2.70\,\mathrm{d}^{-1}$. We first searched for signals in the B and V periodograms in the 23-season composite and found none. However,

we did find a possible weak peak at $2.695\,d^{-1}$ in the 1998–2004 multiseason periodograms, which are shown in Fig. 8a. Their annual sidelodes are also visible. To see if this candidate signal also exists for Season 1997, the season closest to the UV 1996 campaigns, we computed the periodograms for this season and display them in Fig. 8b to show that they have the same peak. Note that although the Season 1997 noise is twice as large as Season 1998-2004, the signal is three times stronger. From these results, the putative signal is weakening and beomes invisible in late APT seasons. Although there is no immediate way of checking, it is possible that in recent years the UV dips have no longer been present.

To verify our Season 1997 detection, we have constructed artificial datasets by estimating the egress wing to the pre-dip level and thus completing the expected UVC curve out to 1.216 days from observation start (see dashed line in Fig. 7). We then repeated and concatenated the curve 115 times until it covered the full span of this season. Since the signal-to-noise of the GHRS greatly exceeded the APT's, we then added Gaussian noise to simulate the APT's data fluctuations. Finally, we sampled the noisy, season-long curve at the actual observation times. We repeated the procedure for various assumed noise levels. The result was a series of mock light curves for various noise levels that retain the observing window gaps.

Figure 8c shows the resulting periodogram for a mock SNR of 250 per observation, which matches the measured APT r.m.s. The position of the generated signal, at $2.697\,d^{-1}$, is already "locked in" to the 8.90 hr we measured earlier, so its position is a given. Similarly, the SNR of the peak height to the surrounding noise level is not unexpected either because the estimated noise level of the observations was determined from the scatter of comparison-check star observations (see §3). However, the near agreement of the simulated and observed peak heights in Figs. 8b & 8c reassures us that the signal is stellar. Because the strengths of the dips are already known to vary over time (e.g., the dips were stronger in 1982), we consider this amplitude agreement fortuitous.

5. DISCUSSION

5.1. *High frequency pulsations and migrating subfeatures*

High-frequency modes are now known to be active in Be stars, e.g., in π Aqr, a γ Cas analog, which exhibits one or more tesseral modes (Nazé et al. 2020b, "N20b"). The amplitudes of these features traveling through line profiles amount to several percent in line profiles (1–2.5 mmag in the optical light curve). In N20b's Fig. 4 one sees that the spacings of the NRP-induced migrating subfeatures in optical spectra of π Aqr, undoubtedly due to high-frequency p-modes, are rather uniformly spaced in time. Thus, there are more differences than similarities in the *msf* of this star's spectrum compared to γ Cas.

In view of the results on π Aqr, we now revisit the Yang et al. (1988) and our own reports of migrating subfeatures in optical and UV spectral profiles of γ Cas. In this context, L20 have doubted our interpretation of these features as clouds forced into corotation over transient magnetic centers on the star (Smith & Robinson 1999). Therefore, we now address arguments for an NRP interpretation for the *msf.*

The most precise record of migrating subfeatures in the spectrum of γ Cas is the 21.5 hr time series of GHRS UV spectra. In this series, a raft of *msf* associated with many lines is ubiquitous. The features traveled across line profiles at a rate of $+95\pm5\,km\,s^{-1}\,d^{-1}$ and reoccur at unpredictable intervals averaging very roughly 2 hours ($12\,d^{-1}$) during this time series. Importantly, they wax and wane in visibility in about $1\frac{1}{2}$ hrs. In a separate study Smith (1995) discussed 109 high-dispersion difference spectra of the He I λ6678 profile during five nights in 1993; each monitoring interval was 3–6 hours. Difference spectra revealed *msf* striation patterns that reoccurred at erratic intervals on most nights and lasted no more than 2-3 hours. The acceleration rate of the features was $+92\pm10\,km\,s^{-1}\,d^{-1}$, in good agreement with the later UV results. Similarly, the unpredictable appearances and short lifetimes of these events render any attempt to measure their recurrences all but meaningless. The cyclical intervals between these patterns averaged 2–$2\frac{1}{2}$ hrs in the 1993 monitoring and $1\frac{1}{2}$–2 hrs for the 1996 UV monitoring. For the following discussion we note that the observed amplitudes of the *msf* were about 0.4% for the optical He I line and (depending on the line's excitation) 0.3–0.6% for the UV, i.e., the *msf* amplitudes are similar in the two wavelength regimes.

With this description, we discuss why high-frequency NRPs are not the best explanation for the *msf* in γ Cas:

1. The absorption features are noncoherent. Also, unlike NRP bumps in line profiles, they are not necessarily most prominent in the middle of their lifetimes.

2. To match roughly the irregular spacings of the *msf* in the GHRS dataset, an NRP p-mode would have a frequency of 9–$12\,d^{-1}$. The reported signal at $7.57\,d^{-1}$ (N20c, LB21) is too low to meet this criterion.

3. Consider that the ratio of line profile-to-photometric *msf* semiamplitudes in π Aqr is 2.5% to 1 mmag.

These variations are due to NRP (Nazé et al. 2020b). Because the amplitudes of *msf* in γ Cas spectra are five times smaller, the photometric amplitudes in γ Cas periodograms should be 0.2 mmag if they too are caused by NRP. Since the TESS periodogram of γ Cas rules out photometric amplitudes down to less than 0.1 mmag at high frequencies, the line profile *msf* of γ Cas are not likely to be caused by NRP.

4. Within measurement errors, the amplitudes of *msf* are the same for optical and UV spectra. This is an important point because the restoring force of high-frequency pulsations is due to pressure imbalances (from their high frequencies they are likely to be p-modes). Model atmosphere simulations indicate that temperature variations from pulsations represented by spherical harmonics cause flux variations in early-type B stars that are $\approx 2\frac{1}{2}$ times as large as in the optical, not equal to them as observed.

Of these arguments, the third one is probably the most powerful. However, the stipulation should be made that the amplitude of the line-profile and photometric *msf* reflected behaviors at different times. The fourth argument relies on the wavelength-dependence of amplitudes in the UV being large compared to optical for high-degree p-modes, as is true for low-degree ones. At least for rapidly rotating, early-Be stars this is relatively unexplored territory, and further exploration is necessary. To date, the amplitude behavior with wavelength seems to have been investigated theoretically so far only up to intermediate-degree (l=3-4), classical g and p modes (e.g., Pigulski et al. 2017).

We remark further that if UV-absorbing structures are suspended over different stellar latitudes, their signatures will exhibit more than one acceleration across the line profiles.

5.2. *The nature of the 0.82 d^{-1} frequency*

As part of our initial justification for assigning f_{82} to rotational modulation, Paper 1 argued that the alternative, classical NRP modes were not likely to be excited in rapidly rotating early-type Be stars, whereas this frequency is quite consistent with rotational modulation of a surface inhomogeneity. As described next, this was likely to be a premature conclusion. In the meantime, various spectroscopic campaigns as well as a flood of results and satellite photometric surveys have shown that nonradial pulsations are endemic to Be stars, including early-type and rapidly rotating stars.

NRP was given a major boost from the study of spectral line profile variations for a small but representative population of other early-type classical Be stars (e.g., Rivinius 2003). More recently, the discovery of groups of frequencies sometimes close to the rotation frequency, Ω_R, has presented evidence that nearly all of them must be due to NRP (Baade et al. 2016). Even so, some investigators (e.g., Balona & Engelbrecht 1986, Balona 1995) have argued that one of these frequencies, particularly if it is visible at intermittent intervals, ean be caused by rotational modulation of a starspot.

Satellite photometry has demonstrated that NRP modes are endemic to early-type Be stars. Recent photometric satellite surveys (e.g., Balona et al. 2015; Semaan et al. 2013, 2018; Saio et al. 2017; Labadie-Bartz et al. 2020; Balona & Ozuyar 2020a,b, "BO20a, BO20b") have disclosed, for most stars exciting low-frequency signals near their rotation rates (Ω_R), that these signals are members of clusters of frequencies, wherein only one at most can be rotational.

Yet, one can ask whether there exist rapidly rotating, early-type Be stars with single isolated frequencies near Ω_R? Balona (2020) reports that in the larger TESS survey of BO20b, five O9–B2 stars exhibit apparent isolated, coherent modes at frequencies that arguably coincide with the rotation frequency. Therefore, because such signals that meet our conditions do exist in a few early-type Be stars, it is now apparent we can no longer hold, as in our previous papers, that the isolated signal at f_{82}, though arguably close to Ω_R, is unique to γ Cas.

Before interpreting the f_{82} frequency as arising from a long-period g-mode, one should consider a potential obstacle. This is that an oscillation observed near f_{rot} in the inertial frame will have a frequency of nearly zero in the corotating frame, i.e., the period will be very long in the (physically important) reference frame. Its corresponding peak in the periodogram would blend with its high-order neighbors, causing a broad peak, which is not observed. A better identification would be of an r-mode, which is an essentially horiontal vorticial pattern at the surface excited by Coriolis force imbalances (or the κ mechanisam Saio et al. (2017)), to which we turn next.

Several years ago Walker et al. (2005) reported the excitation of a thicket of low frequencies ($\lesssim$0.005 mHz) in the rapidly rotating B5e star HD 163868. Unlike several other modes of frequencies 0.02 mHz or higher, which can be ascribed to p or g modes, this low-frequency cluster is close to a multiple of the rotational frquency (i.e., 0.90-0.95mΩ, where perhaps $m = 1$). According to Saio (2013, 2018), these are probably signatures of odd, low azimuthal order r-modes. The circulation of surface par-

ticles participating in r-modes are associated with large polar-direct velocity components at mid-latitude. This renders the discovery of r-modes particularly advantageous in stars observed at intermediate inclination like HD 163868.

Since γ Cas is likewise observed at an intermediate inclination, its f_{82} signal may likewise be due to a low-degree r-mode. Notably, r-modes are predicted to occur as clusters of frequencies, often adjacent to a dominant one (e.g., Walker et al. 2005, Saio et al. 2018). From previous and present APT results, it has appeared to us thus far as if only an isolated peak is visible near f_{82}. If f_{82} is indeed an r-mode, other associated r-modes may be present with amplitudes too small to be detected by the APT. Thus, LB21's detection of multiple low-amplitude g_1 modes in their TESS light curve appears to be consistent after all with f_{82} being the dominant mode of an r-mode complex, at least when it was visible in early years of the APT program. In addition to γ Cas and HD 163868, a few rapidly-rotating B stars in the cluster NGC 3766 may well excite both g- and r-modes (Saio et al. 2017).

5.3. *Extra-APT contributions*

As few in number as the UV satellite monitorings of γ Cas are, combined with the revised ephemeris of Table 3, they permit a reinvestigation and an entry of new evidence as to the origin of the f_{82} signal.

We measured the times corresponding to passages of the centroids of the *first* dip in the IUE 1982, IUE 1986, and GHRS light curve (Fig. 7). These occur respectively at RJD's 44997.48, 50101.57, and 50157.70. According to our Table 3 ephemeris, these times correspond to faint-star phases 0.41, 0.92, and 0.08, respectively. We estimate errors on the 1996 IUE and GHRS phases as $\pm$0.02 and $\pm$0.03. These values are dominated by errors in our adopted frequency (Table 3). For the more important *phase-difference* error between the two 1996 first-dip centroids (the time interval being 57 days), the error in the frequency is negligible. The error in the 1996 IUE feature relative to the GHRS feature is dominated by centroid measurement and is $\pm$0.02. The errors for the 1982 IUE dip are larger, $\pm$0.05, because the frequency and centroid-finding errors must be folded together. Similarly, phases for the centroids of the *second* UV dip are 0.71, 0.22, and 0.39. We estimate phase errors in the GHRS second dip to be dominated by uncertainty in frequency, whereas errors in the IUE second-dip centroids are about 50% larger because their profiles are not as well defined. If we had instead adopted the B20 frequency and our $T_\circ$ from Table 3, the phases would be different, but the net result is much the same. All told, the far-UV features are not phase-locked with the optical ephemeris. The phasing mismatch occurs even over the small interval (46.16 cycles) in the $\approx$57 day interval between the 1996 IUE and GHRS observations. Assuming a cycle miscount of 0 or 1, the percentage mismatch would be either 0.4% or 2.5%, respectively, which, though small, introduces a phase slippage.

The resolution of this slippage starts with the fact that only one frequency can be rotational. We believe it is unrealistic that, over the 57 day interval between 1996 IUE and GHRS observations, a surface differential rotation rate of order 1% or more occurs. Therefore, we reject this possibility. It follows that we *prefer* to adopt the alternative: f_{82} is not a rotational signal. Yet, our preference does not prove the case. In fact, given the isolation of the signal at low frequency and its sometime nonsinusoidal waveform, the identification of f_{82} with NRP is not straightforward. In any case, in view of the arguments put forth regarding the UV color changes of the dips (SRH) and the correlation of appearances with changes in UV spectral lines and hard X-ray flux (SLM16), we can see no reason to reject the co-rotating picture. This does not mean that the rotation frequency has been found. Given the physical parameters of the star and the likely reoccurrence of the "first dip" in the 1982 IUE light curve, it is probably near $0.8\,\mathrm{d}^{-1}$.

6. SUMMARY AND CONCLUSIONS

We summarize the main points of this work as follows:

* The discovery of coherent signals with frequencies at 1.24, 2.48, and $5.03\,\mathrm{d}^{-1}$ found by B20 or N20c has been confirmed by an independent dataset (APT).

* We agree with previous authors that these signals are NRP (p- or low-degree g-) modes. These modes should not be confused with the stochastic low-frequency ($\sim 0.1-2\,\mathrm{d}^{-1}$) variability discovered in a variety of OB stars in TESS data (e.g., Bowman et al. 2020). For early B stars the amplitude of such "white noise" is generally only $\sim$0.1 mmag in B III-V stars and thus is well below the detection limit of the APT. This variablity is thought to be excited by turbulence generated within the Fe-opacity convective zone (e.g., Cantiello et al. 2021).

* The $0.82238\,\mathrm{d}^{-1}$ frequency was stable in B, V filters from 1997 through 2011, although the amplitude varied. Since then, the signal has faded and then showed a weak recurrence (2014-2016). We cannot verify that it was active during 2017-2019.

* NRP amplitudes can at times wax and wane rapidly. Such activity is also displayed in N20c's TESS dynamic periodogram and Fig. 9.

* We believe the $0.82\,\mathrm{d}^{-1}$ signal is an excited NRP mode of still undetermined type. However, its occasional tendency to modify its waveform complicates a physical description of its origin. Also, the isolated position of a detectable signal near Ω_R (but how near?) may not be unique among early Be stars (BO20b), but it is not the norm either. Otherwise, given the excitation of these modes, γ Cas has begun to resemble other Be stars at the periphery of the β Cep domain.

* Our preference for attributing the cause of f_{82} to NRP rather than rotational modulation was facilitated by using UV light curves. These indicate phase shifts from our f_{82} ephemeris. We identify the pair of dips from UV photometry as being likely due to rotation. However, because we do not know the putative stellar longitude separations of the absorbing structures, we cannot determine the exact value of Ω_R.

* In periodograms of early APT season data we found a signal at $2.70\,\mathrm{d}^{-1}$ that corresponds to the time separation of the two-dip pattern observed in the three UV campaigns of 1982 and 1996. However, periodograms of (most) later APT seasons and recent satellite datasets do not exhibit this signal. We conclude that it has diminished and may no longer be visible in the UV or optical.

* TESS data offer no evidence that high-frequency NRP modes produce the migrating subfeatures in optical and UV spectra of γ Cas. Moreover, the *msf* are chaotic, exhibit much larger amplitudes than the APT and TESS detection thresholds, and do not show an expected increase in amplitude from the optical to far-UV.

* The so-called long cycles abruptly faded to invisibility just after the era covered by Paper 2 and shortly after the 2010 outburst. (A possible recovery in two recent seasons might have occurred, Fig. 2, but is too weak to be reliable.) We speculate that the continued build-up of the inner disk, according to APT photometry and especially the increased He I λ6678 emission (Pollmann et al. 2014) is caused by an increased density there that overwhelms a fragile disk dynamo mechanism.

* The correlation of APT and X-ray long cycles argues that the Be disk mediates the production of hard X-rays on the star. Optical variations found by the APT have therefore been important in framing the magnetic interaction hypothesis.

In criticizing the star-disk magnetic interaction hypothesis, L20 and B20 overlooked some key points. The existence of the f_{82} signal is largely irrelevant to the production of hard X-ray flux in this picture.[2] The spectral *msf* are supportive though not essential to the basic picture unless they can be identified with large X-ray "flares." However, if instead they turn out to be due to high-frequency NRPs after all, the case for suspended *cloudlets* would disappear. The optical/X-ray long-cycle connection *is* important to the picture – the previous points are not required. The high densities associated with the flares strongly suggest a photospheric origin, to say nothing of the correlation of hard X-ray fluxes with photospheric UV line strengths (SR99). Therefore, any rapid, aperiodic events, e.g., caused by emerging magnetic structures, should be examined as aiding in the understanding of the X-ray formation process.

ACKNOWLEDGMENTS

This study would not have been possible without the support of Lou Boyd, who has conscientiously managed the automatic telescopes at Fairborn Observatory. We are indebted to Drs. Yael Naze, Gregor Rauw, Andrzej Pigulski, and Mr. Piotr Kolaczek-Szymanski for sending us satellite light curve extractions of γ Cas and for many suggestions that improved the manuscript. We are also grateful to Drs. Raimundo Oliveira de Lopes and Christian Motch for comments on the draft. It is a pleasure to acknowledge an anonymous referee's calling our attention to an important error in an earlier version of the manuscript and for many insightful suggestions. GWH acknowledges long-term support from NASA, NSF, Tennessee State University, and the State of Tennessee through its Centers of Excellence Program.

REFERENCES

[2] The rotation rate comes into the discussion of details of corotating clouds, and then only secondarily in estimating their elevations. As such the error in equating f_{82} to Ω_R cannot be large.

Baade, D., Rivinius, Th., Pigulski, A., et al. 2016, A & A, 588, 56B
Baade, D., Pigulski, A., Rivinius, A., et al. 2018, A & A, 610, 70B
Balona, L. A., 1995, MNRAS, 277, 1547B
Balona, L. A. 2020, priv. commun.
Balona, L. A., Baran, A. S., Dasyńska-Daszkiewicz et al. 2015, MNRAS, 451, 1445B
Balona, L. B., & Engelbrecht, C. A. 1986, MNRAS, 219, 131B
Balona, L, B., & Ozuyar, D. 2020, MNRAS, 493, 252B (BO20a)
Balona, L, B., & Ozuyar, D. 2020, arXiv:2008.06288v1 (BO20b)
Barry, D., Holberg, J. B., Forrester, W. T., et al. 1984, 281, 755B
Borre, C. C., Baade, D., Pigulski, A., et al. 2020, A&A, 635A, 140B (B20)
Bowman, D. M., Burssens, S., Simón-Díaz, et al2020, A&A, 640, A36
Cantiello, M., & Braithwaite, J. 2011, A&A, 540A, 140C
Cantiello, M., Lecoanet, D., Jermyn, A. S. 2021, arXiv:2102.05670v2
Doazan, V., Franco, M., & Sedmak, G. et al.1983, A & A, 171, 180D
Eaton, J. A., Henry, G. W., & Fekel, F. C. 2003, ASSL, 288, 189E
Gies, D. R., Bagnuolo, W. G., Ferrara, E. C., et al. 1998, APJ, 493, 440G
Hamaguchi, K., Oskinova, L., Russell, C., et al. 2016, ApJ, 832, 140H
Harmanec, P. 2002, Exotic Stars, ed. Tout, C. & Van Hamme, W., ASP Conf. Ser., 279, 221M
Harmanec, P., Habuda, P., Stefl, S., et al. 2000, A & A, 364, L85H
HEASARC Rosat_Data_Archive 2020, https://heasarc.gsfc.nasa.gov/docs/cgro/db-perl/W3Browse/w3table.pl
Henry, G. W. 1995a, in ASP Conf. Ser. 79, Robotic Telescopes, ed. G. W. Henry & J. A. Eaton (San Francisco: ASP), 37H
Henry, G. W. 1995b, in ASP Conf. Ser. 79, Robotic Telescopes: Current Capabilities, Present Developments, and Future Prospects for Automated Astronomy, ed. G. W. Henry & J. A. Eaton (San Francisco: ASP), 44H
Henry, G. W. 1999, PASP, 111, 845H
Henry, G. W. & Smith, M. A. 2012, ApJ, 760, 10H (Paper 2)
Labadie-Bartz, J., Carciofi, A. C., Henrique de Amorim, T., et al. 2020, arXiv:2010.139055v1
Labadie-Bartz, J., Baade, D., Carciofi, A. C. et al., MNRAS, 502, 242L, 2021 (LB21)
Langer, N., Baade, D., Bodensteiner, J., et al. 2020, A & A., 633A, L40 (L20)
Mamajek, E. 2017a, J. Double Star Obsns., 2, 264M
Mamajek, E. 2017b, priv.commun.
Markwardt, C. 2011, Markwardt IDL Library, https://pages.physics.wisc.edu/∼craigm/idl/idl.html
Mason, K. O., White, N. E. & Sanford, P. W. 1976, Nature, 260, 690M
Motch, C., Lopes de Oliveira, R., & Smith, M. A. 2015, ApJ, 806, 177M
Murakami, T., Koyama, K., Inoue, H., et al. 1986, ApJ, 310, L31M
Nazé, Y., Motch, C., Rauw, G., et al. 2020a, MNRAS, 493, 2511N (N20a)
Nazé, Y., Pigulski, A., , Rauw, G., et al. 2020b, MNRAS, 494, 958N (N20b)
Nazé, Y., Rauw, G., & Pigulski, A. 2020c, MNRAS. 498, 3171N (N20c)
Nemravová, J., Harmanec, P., Koubska, P., et al. 2012, A&A, 537, 59-69N
Peters, G. J., Gies, D. R., Grundstrom, E. D., et al. 2008, 686, 1280P
Peters, G. J., Pewett, T. D., Gies, D. R., et al. 2013, ApJ, 765, 2P
Peters, G. J., Wang, L., Gies, D. R., et al. 2016, ApJ, 828, 47P
Pigulski, A., Baran, A., Bzuowski, M., et al. 2017, Proc. Polish Astron. Soc., Vol 5 ed. K. Zwintz & E Poretti, 76P
Pollmann, E., Vollmann W., & Henry, G. W. 2014, IAU Info. Bull. No. 6109, #1
Pollmann, E., et al. 2021, JAAVSO, 49, No. 1
Postnov, K., Oskinova, L., & Torrejón, J. M. 2017, arXiv:2017.00336v1
Ricker, G. R., Winn, J. N., Vanderspek, R., et al. 2015, J. Astr. Telescopes, Instr. & Syst, Vol. 1, id 014003
Rivinius, Th., Baade, D., & Stefl, S. 2003, A & A, 411, 229R
Robinson, R. D., & Smith, M. A. 2000, ApJ, 540, 474R (RS00)
Robinson, R. D., Smith, M. A., & Henry, G. 2002, ApJ, 575, 435R (RSH)
Saio, H. 2013, Lect. Notes Phys. "Seismology for Studies of stellar rotation," ed. K. Belkacem, 835, 3M.
Saio, H., Ekström, S., Mowlavi, N. et al. 2017, MNRAS, 467, 3864S
Saio, H. 2018, Proc. Physics of Oscillating Stars Conf., arXiv:1812.01253

Semaan, T., Hubert, A. M., Zorec, J. et al 2013, A&A, 551, 130SS

Semaan, T., Hubert, A. M., Zorec, J. et al 2018, A&A, 617, A70SS (Sem18)

Smith, M. A. 1995, ApJ, 442, 812s

Smith, M. A. 2019, PASP, 131, 4201S (S19)

Smith, M. A., Henry, G. W., & Vishniac, E. 2006, ApJ, 647, 1375 (Paper 1)

Smith, M. A., Lopes de Oliveira, R., & Motch, C., et al. 2012, A&A, 540, A53S (SLM)

Smith, M. A., Oliveira, R., Motch, C. 2016, ASpR, 58, 782S (SLM2016)

Smith, M. A., & Robinson, R. D. 1999, ApJ, 517, 866S (SR99)

Smith, M. A., & Robinson, R. D. 2003, Interplay of periodic, cyclic, & stochastic variability, ed. C. Sterken, ASP Conf. Ser. 292, 263S

Smith, M. A., Robinson, R. D., Corbet, R. H. 1998a, ApJ, 503, 877S (SRC)

Smith, M. A., Robinson, R. D., Hatzes, A. P. 1998b, ApJ, 508, 945S (SRH)

Vaníček, P. 1971, Ap&SS, 12, 10V

Walker, G. A., Kuschnig, R., Matthews, J. M., et al. 2005, ApJ, 635. L77W

Wang L., Gies, D. R., & Peters, G. J. 2017, ApJ, 843, 60W

Wang L., Gies, D. R., & Peters, G. J. et al. 2021, arXiv:2103.13642v1

White, N. E., Swank, J. H., Holt, S. S. 1982, ApJ, 263, 277W

Yang, S., Ninkov, Z., & Walker, G. A. H. 1988, PASP, 100, 233Y